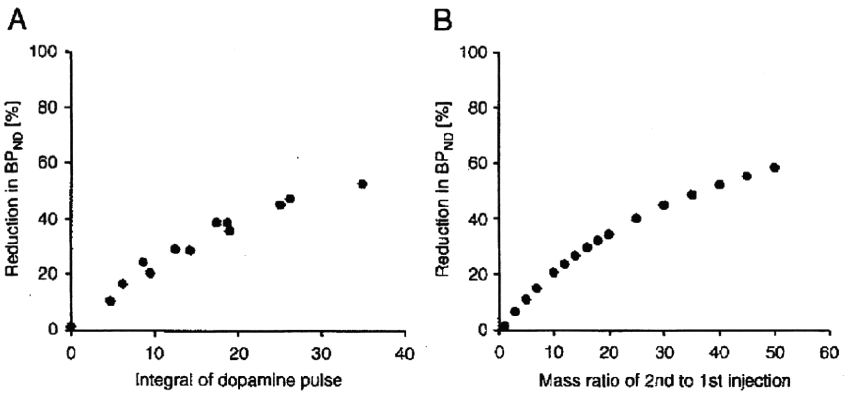

Fig. 2. Relationship between percentage reduction in BP_{ND} and the integral of the dopamine pulse in simulation studies in which dopamine was released at the same time as the second injection, performed 30 min after first injection (A); and the relationship between percentage reduction in BP_{ND} and the mass of the second injection in simulation studies in which a greater mass of raclopride was administered 30 min after the first injection.

onset, magnitude of amplitude, and decay rate of the dopamine pulse, and the reduction in BP_{ND} was greatest when the dopamine pulse was released 5 min after the second injection (Fig. 3C). When the magnitude of the dopamine pulse was small, the detected BP_{ND} reduction was small when the dopamine pulse was released before the second injection, becoming greatest (about 20%) when the pulse was released 5 min or 10 min after the second injection. When the magnitude of the pulse was medium, the BP_{ND} reduction was 20% when the pulse was released 5 min before the second injection, and it was greatest (about 35%) when the pulse was released 5 min after the second injection. When the dopamine pulse was large, the detected BP_{ND} reduction was 30% even when the pulse was released 10 min before the second injection, and was greatest (about 45%) when the pulse was released 0 or 5 min after the second injection.

In the simulation with prompt BP_{ND} reduction, BP_{ND1}, BP_{ND2} and ΔBP were estimated precisely by the MI-SRTM when the BP_{ND} reduction occurred at 30 min, in other words, at the same time as the second injection (Fig. 4). In the case where the BP decreased before 30 min, the estimated BP_{ND1} was lower than the true value for BP_{ND1} (=2.2), and the magnitude of the underestimation increased when the true BP_{ND2} was lower, that is to say, the reduction in BP_{ND} was greater (Fig. 4A). There were slight errors in BP_{ND2} estimates (Fig. 4B). When the BP_{ND} decreased 50% ($BP_{ND1}=2.2$ and $BP_{ND2}=1.1$) at 10 min before the second injection, estimated BP_{ND1} was 1.63 and BP_{ND2} was 1.04. Conversely, when the BP decreased after 30 min, BP_{ND1} was estimated precisely, and BP_{ND2} was overestimated (Figs. 4A and B). The error in BP_{ND2} estimates increased as the magnitude of the BP_{ND} reduction increased. When the BP_{ND} decreased 50% ($BP_{ND1}=2.2$ and $BP_{ND2}=1.1$) at 10 min after the second injection, estimated BP_{ND1} was 2.20 and BP_{ND2} was 1.28. With respect to the magnitude of the BP reduction, the estimated ΔBP was lower than the true value when the BP reduction was greater, or the difference between the timing of the BP_{ND} decrease and the second injection was greater (Fig. 4C). When the BP_{ND} reduction began 10 min before the second injection, the error in the estimated ΔBP was considerable. However, when the BP_{ND} reduction began, either 5 min before or 5 min after, the second injection, the error in ΔBP was less than 5% when the reduction in the BP was lower than 50%.

Effect of injection interval on BP_{ND} estimates

Errors in the estimated BP_{ND1}, BP_{ND2} and ΔBP values were investigated in simulated noise-added TACs for various injection intervals, and it was observed that the errors became larger as the injection interval became shorter (Fig. 5). The COVs of BP_{ND1} and BP_{ND2} were less than 5% and the bias was less than 1% when the injection interval was longer than 30 min, in both cases where the reduction in the BP_{ND} was 30% and 70%. When ΔBP was 30%, the bias increased suddenly, and the COV of ΔBP rose to over 10% for an injection interval of less than 40 min. There were no outliers even if the injection interval was 20 min. Meanwhile, when ΔBP was 70%, there was little bias and the COV of ΔBP was less than 10% for an injection interval longer than 30 min. The COV of ΔBP in the 70% reduction TAC was lower than that in 30% reduction TAC. However,

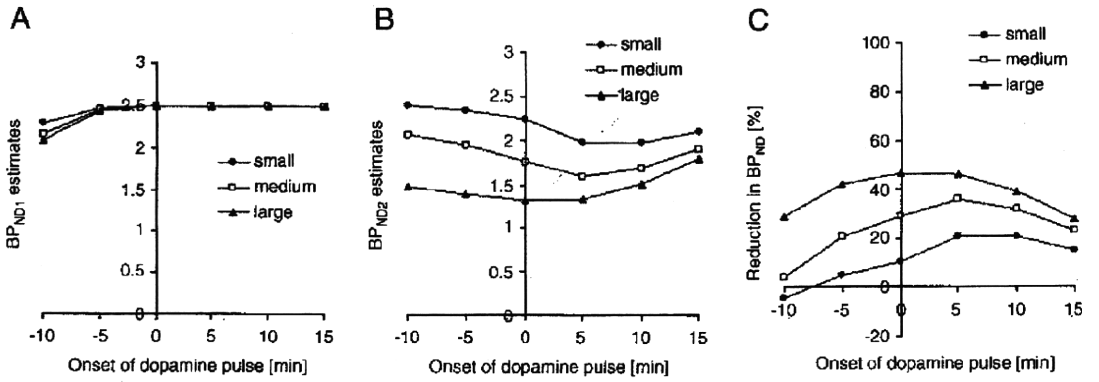

Fig. 3. Relationship between estimated values of BP_{ND1} (A), BP_{ND2} (B), reduction in BP_{ND} (C) and the onset of the dopamine pulse, in simulation studies with a small pulse ($H=0.5$, $R=0.1$), medium pulse ($H=1.0$, $R=0.07$), and large pulse ($H=1.5$, $R=0.04$) released −10, −5, 0, +5, +10, or +15 min with respect to the second injection.

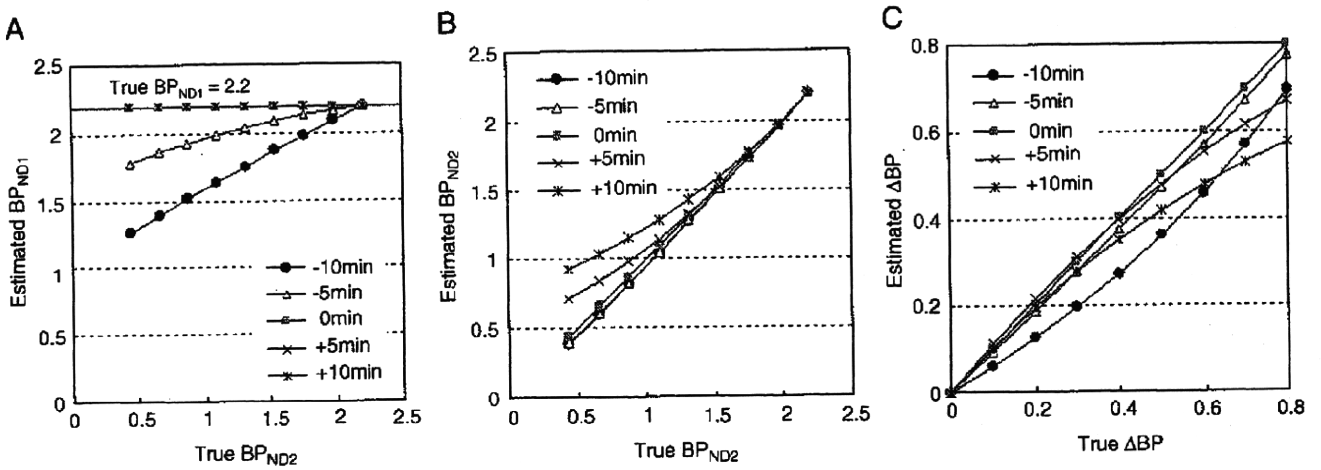

Fig. 4. Relationship between estimated values of BP_{ND1} (A), and BP_{ND2} (B) and the true values of BP_{ND2}, and the relationship between the estimated reduction in BP_{ND} (ΔBP) and true ΔBP (C) in the simulation studies in which BP_{ND} changed promptly from 2.2 to the true BP_{ND2} at −10, −5, 0, +5, or +10 min, with respect to the second injection.

there were 22 outliers with unreasonable estimates when the injection interval was 20 min and one outlier in one thousand estimates when the injection interval was 30 min.

Monkey studies

Typical examples of TACs for the striatum and the cerebellum in the dual-injection study with the same amount of raclopride are shown in Fig. 6. In these studies, the BP_{ND} values for the first and second injections could be estimated, and there were little differences between BP_{ND1} and BP_{ND2} (Table 2).

Time–activity curves for the striatum and the cerebellum in the dual-injection study using different amounts of raclopride are shown in Fig. 7, and the parametric images of BP_{ND1} and BP_{ND2} are shown in Fig. 8. The estimated BP decreased when the binding changed at the second injection due to the addition of more raclopride than was

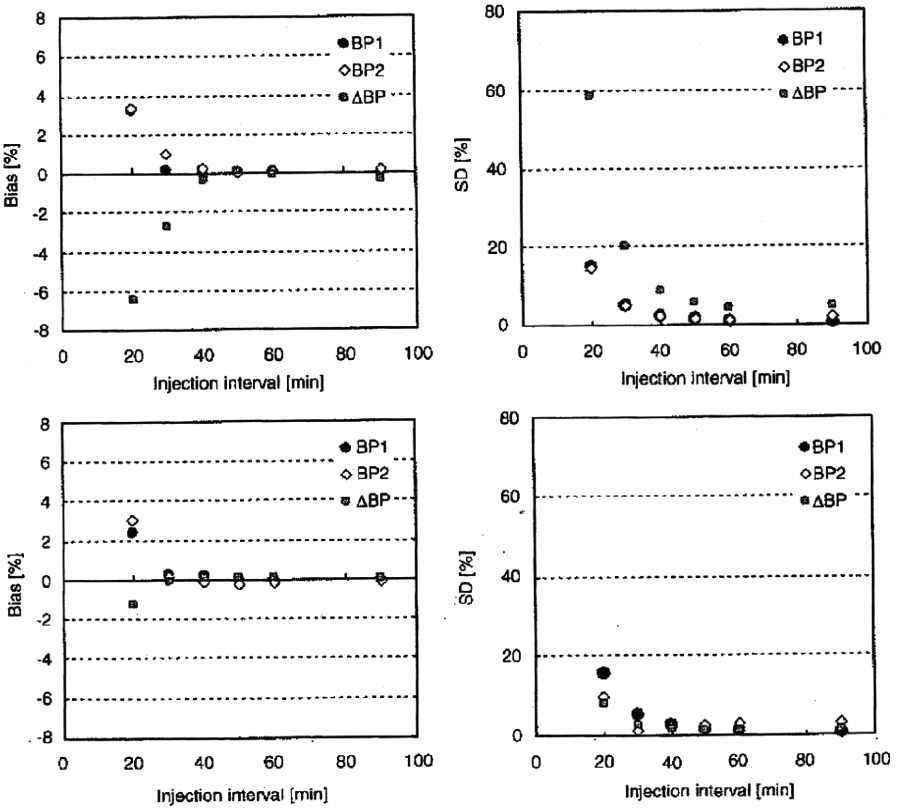

Fig. 5. Relationship between the injection interval and bias (left) or SD (right) of BP_{ND1}, BP_{ND2}, and the reduction in BP_{ND} (ΔBP) when BP_{ND} decreased by 30% (upper) or 70% (lower) at the time of second injection.

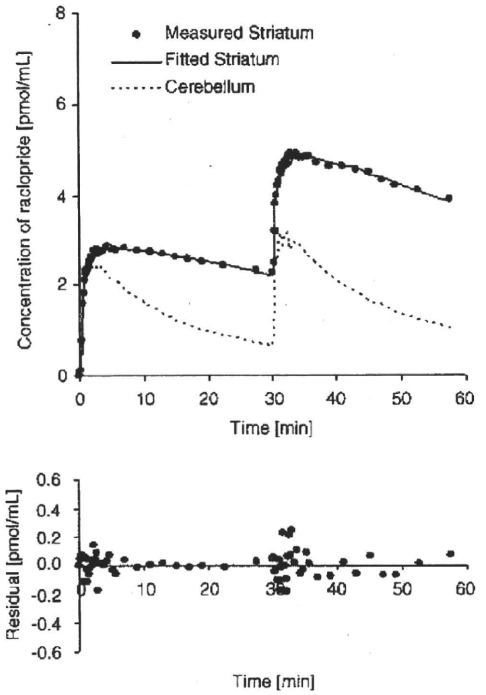

Fig. 6. Measured time–activity curves of the striatum and cerebellum in the dual-injection study with the same mass of [^{11}C]raclopride and a fitted curve for the striatum, using the multiple-injection SRTM (upper), and residuals between measured and fitted curves (lower).

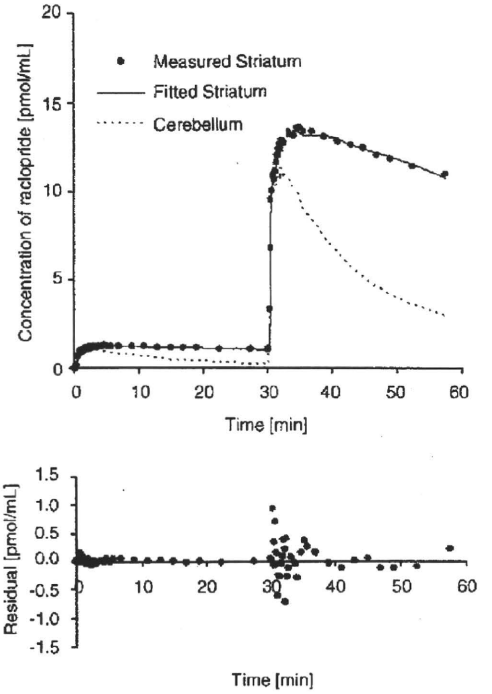

Fig. 7. Measured time–activity curves of the striatum and cerebellum in the dual-injection study with a different mass of [^{11}C]raclopride and a fitted curve for the striatum, using the multiple-injection SRTM (upper), and residuals between measured and fitted curves (lower).

administered for the first injection. Estimated BP_{ND1}, BP_{ND2} and ΔBP values in the striatum were 2.7, 2.0, and 25%, respectively (Table 2). The reduction in BP_{ND} was also observed in the parametric images as shown in Fig. 8.

Discussion

In the competition paradigm, the binding potential of [^{11}C] raclopride reflects the condition of specific binding to dopamine D_2 receptors, which is affected by competition with other ligands if there are no changes in the density of the receptors. The SRTM can provide the BP_{ND} value without invasive arterial blood sampling, using a TAC of the reference region, where specific bindings are negligible (Lammertsma and Hume, 1996), and this method has been widely used to estimate the binding of neuroreceptor ligands. However, in assessing temporal changes in the BP_{ND} of the SRTM caused by competition for receptor binding due to pharmacological administration or cognitive activation, multiple [^{11}C]raclopride PET scans are necessary and a long study period is required. To overcome this complication, we have proposed a multiple-injection approach in which the temporal change in BP_{ND} is quantified in a single scan with multiple [^{11}C]raclopride injections. This approach takes into account the residual radioactivity from the first injection in the target tissue, at the time of the second injection, as the initial condition in Eq. (2), and makes it possible to perform the second injection immediately, following data acquisition from the first injection. Thus it is possible to determine the change in BP_{ND} from a short study period.

There have been several investigators who attempted to perform multiple injections of ligands with PET studies for either obtaining receptor density and affinity by changing specific activity (Delforge et al., 1995; Millet et al., 1995; Morris et al., 1996a,b; Muzic et al., 1996; Christian et al., 2004; Gallezot et al., 2008), or obtaining different kinetic parameters simultaneously by injecting different tracers such as [^{11}C]flumazenil and [^{18}F]FDG (Ikoma et al., 2004; Koeppe et al., 2001). MI-SRTM gives us alternative approach for multiple-injection study which is aimed at shortening study period.

Table 2
Estimated BP_{ND1}, BP_{ND2}, and difference between BP_{ND1} and BP_{ND2} in monkey studies with dual injections of [^{11}C]raclopride.

	Subject	BP_{ND1}	BP_{ND2}	ΔBP
	#1	1.86	2.15	0.15
	#2	1.98	2.01	0.014
Exp. 1	#3	1.95	1.79	−0.081
	#4	2.33	2.39	0.027
	mean ± SD	2.03 ± 0.20	2.08 ± 0.25	0.029 ± 0.097
Exp. 2	#5	2.66	2.00	−0.25

$\Delta BP = (BP_{ND2} - BP_{ND1}) / BP_{ND1}$.
Exp. 1: Dual injections with same mass of [^{11}C]raclopride.
Exp. 2: Dual injections with different mass of [^{11}C]raclopride.

Detection of binding changes with the SRTM

In the multiple-injection approach, it is assumed that the change in binding conditions is reflected by a reduction in BP_{ND} estimated from the SRTM. The analysis method based on the compartment model assumes that the rate constants of K_1 to k_4 are constant during the scan. However, in studies with changes in binding conditions, levels of endogenous dopamine change after exposure to stimuli such as an amphetamine challenge (Endres et al., 1997; Laruelle et al., 1997), and the value of $k_3'(t)$ in Eq. (3) varies according to the concentration of free dopamine (Laruelle et al., 1997, Endres et al., 1997). Therefore, estimates of BP_{ND} following exposure to stimuli are considered to be an average value over time that is influenced by the dynamics of the neurotransmitter. However, it has been reported that reductions in BP_{ND}, estimated from graphical analysis or multilinear analysis, in simulation studies for two separate bolus-injection scans, are related to the integral of dopamine release (Endres and Carson, 1998; Yoder et al., 2004), and the reduction in BP_{ND} is a useful index for the evaluation of binding conditions in competition paradigms.

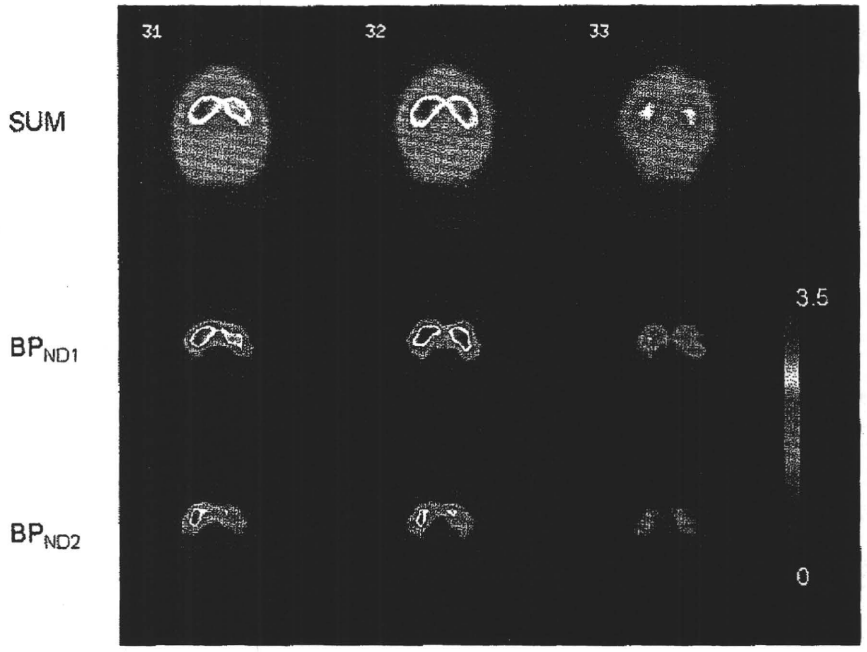

Fig. 8. Summation image and parametric images of BP_{ND1} and BP_{ND2} in the monkey study with dual injections of different masses of [^{11}C]raclopride.

In addition, in the SRTM, there are further assumptions that the target tissue and reference tissue can be expressed by a one-tissue compartment model, and the ratio of K_1 and k_2 are equal between the target and reference regions (Lammertsma and Hume, 1996). Strictly speaking, this assumption does not apply to [^{11}C]raclopride studies because significantly better fits were obtained with a two-tissue compartment model, as compared with those obtained with a one-tissue compartment model in cerebellum and striatum TACs (Lammertsma et al., 1996). Therefore, this assumption of the SRTM induces a bias in BP_{ND} estimates even in an ordinary single-injection study. In the MI-SRTM, which is an extension of the SRTM, the effect of the assumption could be more severe than for the SRTM because the bias in BP_{ND1} could be propagated to the estimation of BP_{ND2}. However, in our simulation studies, the ΔBP_{ND}, estimated from the MI-SRTM, increased according to the increase in the dopamine pulse or to administered raclopride (Fig. 2). When the specific binding of administered [^{11}C]raclopride competed with that of endogenous dopamine, to some extent the reduction in BP increased in proportion to the integral of the released dopamine pulse, and approached saturation as the integral of the pulse increased. This is consistent with results reported in previous studies (Endres and Carson, 1998, Yoder et al., 2004). Furthermore, in the monkey studies, it was confirmed that there was little change in BP_{ND} when the same mass of raclopride was administered for the first and second injections (Fig. 6), and the BP_{ND} decreased in accordance with the increase in administered raclopride (Figs. 7 and 8). Morris et al. (1996b) intensively investigated the characteristics of multiple injections PET studies, and they showed varied specific activity by multiple injections introduced bias in estimates of kinetic parameters. Our results may be influenced by the abrupt discontinuity in mass of raclopride due to the second injection. However, the result of second monkey study (10 times higher mass in the second injection) agreed well with the simulation (Fig. 2B) although further validation studies will be needed to confirm this result.

Effect of binding change timing on BP_{ND} estimates

In estimating the BP_{ND} after the dopamine pulse release, the timing of the [^{11}C]raclopride injection has been shown to affect the BP_{ND} estimates (Yoder et al., 2004). In the simulation study of our multiple-injection approach, BP_{ND1} (in other words, the BP_{ND} for the condition without dopamine activation) had few errors, except when the dopamine pulse was released 10 min before the second injection. In these simulations, BP_{ND1} was estimated using the data from the time interval between the first injection and the second injection. Therefore, when the BP_{ND} reduction, due to an increase in free dopamine, started before the second injection, the value for BP_{ND1} was underestimated. However, this underestimation can be avoided by adjusting the data points used for the fitting of BP_{ND1} so that BP_{ND1} is determined before a change in the binding conditions. On the other hand, BP_{ND2}, (that is to say, the BP_{ND} of the condition with dopamine activation) was affected by the timing of the dopamine pulse release. The estimated BP_{ND2} decreased as the onset of the dopamine pulse occurred later, and was smallest when the dopamine pulse was released 5 min after the second injection. As a result, the magnitude of ΔBP was greatest when the dopamine pulse was released 5 min after the second injection.

The value of $k_3'(t)$ in Eq. (3) depends upon the amount of free dopamine at time t (Endres et al., 1997, Endres and Carson, 1998) and the released dopamine pulse decreases as time goes by. Therefore, if the specific activity of administered [^{11}C]raclopride is high enough, the time-varying binding potential ($BPs(t) = k_3'(t)/k_4$) is lowest at the time of the pulse release, and it becomes greater, and approaches the level before the pulse release, as time passes. Meanwhile, the reduction in BP_{ND} is determined by both the $BPs(t)$ and the concentration of free tracer (Endres and Carson, 1998). In the TACs from our simulation studies, the concentration of free [^{11}C]raclopride had a peak at about 5 min after the injection, and ΔBP_{ND} was greatest when the onset of the dopamine pulse occurred 5 min after the injection, as shown in Fig. 3C. Therefore, the reduction in BP_{ND} was greatly affected, not only by the magnitude of the dopamine pulse, but also by its timing. In other words, if the kinetics of the free tracer are similar, that is to say the value of k_2 does not change markedly, and the timing of the dopamine release is the same, the estimated ΔBP changes according to the integral of the dopamine pulse as shown in Fig. 2.

In the situation where BP_{ND} changed promptly, the ΔBP_{ND} also depends upon the magnitude and timing of the BP_{ND} reduction. However, when ΔBP_{ND} was less than 40% and the time difference

between the binding change and second injection was within 5 min, the effect of the timing of the BP_{ND} reduction was slight.

Interval between the dual injections

In the simulation study with noise for the ROI-based estimation, a dual-injection scan with a 30 min injection interval, gave unbiased and reliable BP_{ND1} and BP_{ND2} estimates (Fig. 5). In the 70% reduction TAC, the COV of ΔBP_{ND} was less than 5% when the injection interval was 30 min. Conversely, results from the 30% reduction TAC showed that a 50 min interval would be required to estimate ΔBP_{ND} within a 5% COV. In this study, we evaluated the reliability of BP_{ND} estimates for an ROI-based estimation. However, in voxel-based estimations, the noise level is usually higher, so the COV of estimates can be expected to increase.

In the ROI analysis of human study with single injection, it is reported that a 30 min scan of [^{11}C]raclopride gave unbiased and reliable BP_{ND} estimates (Ikoma et al., 2008). The kinetics of [^{11}C]raclopride in the human brain is different from that in the monkey brain, inducing the difference in required scan durations. The required injection interval for a reliable estimation depends on the kinetics of the ligand, the magnitude of ΔBP_{ND} and the noise level according to injection dose, ROI size, sensitivity of the measurement system, and so on. Therefore, evaluating the effect of the injection interval on the reliability of parameter estimates is important.

Monkey studies

In the simulation studies, it was demonstrated that the MI-SRTM approach could detect a change in BP_{ND} caused by the release of a dopamine pulse or by the increase in administered raclopride. Furthermore, we demonstrated the validity of the proposed method using actual data from monkeys. As a result, the estimated BP_{ND} reduction changed according to the injected mass of raclopride in the second injection, and this is consistent with the results from the simulation studies. We are planning further studies on monkeys with co-injection of various amount of cold raclopride to examine the relationship between the observed changes in BP_{ND} and the occupancy of receptors. Furthermore, using the present approach, it may be possible to estimate endogenous dopamine release by pharmaceutical stimuli although the interpretation of the results must be made with caution because the level of endogenous dopamine is sensitive to the timing and the response of pharmaceutical manipulation (Yoder et al., 2004).

Potential of the multiple-injection approach

The dual-injection approach is able to assess the change in BP_{ND} for receptor competition studies in a single PET scan and shortened study period, as compared to a conventional approach. However, this approach requires some caution. Firstly, the error due to residual radioactivity at the time of the second injection may affect the reliability of BP_{ND2} estimates. Therefore, we estimated the residual radioactivity, not from the measured TAC, but from a fitted TAC from the first injection. In the simulation study, with noise-added TACs, the bias and COV of BP_{ND2} estimated from the second injection were acceptable (Fig. 5).

Secondly, the administered molar amount of second injection must be same as that of the first injection for the evaluation of dopamine release, because the value of BP_{ND} decreases according to the increase in administered raclopride even if the dopamine pulse does not be released (Fig. 2B). In addition, in the dual-injection study, the radioligand for the first injection remains in the tissue at the time of second injection. Therefore, the molar amount of administered raclopride needs to be sufficiently small, that is to say, the specific activity of administered [^{11}C]raclopride should be high enough. The mass of first injection is required to be less than about 1 nmol/kg so that the remained raclopride at the second injection does not affect BP_{ND2} estimates (data not shown). To keep the amount of administered raclopride below 1 nmol/kg with the administration of 37MBq/kg [^{11}C]raclopride, its specific activity should be greater than 37 GBq/μmol. However, in the multiple-injection study, if one can synthesize [^{11}C]raclopride with high specific activity, it is an advantage that [^{11}C]raclopride, synthesized once before the scan, can be administered for both the first and second injections.

Thirdly, the timing of the second injection affected the BP_{ND} estimates, as it was also observed in the estimations using two separate conventional scans. The timing of the second injection should be fixed within the intersubjects of the group, and the interpretation of the ΔBP_{ND} requires some caution when a time–activity curve of free [^{11}C]raclopride differs. The competition paradigm also should be applied carefully in case where the dopamine released slowly in response to stimuli, because it is often difficult to estimate the timing of the dopamine peak. Despite this, we have shown that the multiple-injection approach can be used to determine a reduction in BP_{ND} values as effectively as using two separate scans, but within a single scan lasting 100 min.

The ESRTM approach can also provide ΔBP_{ND} values from a single-session scan by administering [^{11}C]raclopride using a bolus-plus-continuous (B/I) infusion approach (Zhou et al., 2006). Meanwhile, with the MI-SRTM approach, [^{11}C]raclopride can be administered several times by bolus injection, so there is no need to control the administered dose continuously, and it is easy to change the administered mass of raclopride significantly during the scan.

Since the MI-SRTM is a successor of SRTM, one advantage of the MI-SRTM is that the BP_{ND} parametric map can be obtained as shown in Fig. 8, which is crucial to perform statistical parametric mapping (SPM) type analysis. The results of our simulation and monkey studies suggest that the MI-SRTM can be applied to the estimation of ΔBP_{ND} for human study, though the optimal injection protocol needs to be evaluated. One application of the MI-SRTM approach for the human study is to estimate occupancy within short period. By the MI-SRTM approach, one can estimate the BP_{ND} value without antipsychotics and BP_{ND} with antipsychotics from one session of PET study. This approach is also useful in the estimation of receptor density (B_{max}) and affinity (K_d) that normally requires several scans with variable masses of raclopride injections (Farde et al., 1986; Doudet et al., 2003). Furthermore, this approach can be applied to other PET ligands if the BP_{ND} can be estimated by the SRTM approach.

In summary, we have developed a method for estimating the change in binding potential in a single PET scan using multiple injections of [^{11}C]raclopride and a simplified reference tissue model. Our simulations showed that the reduction in BP_{ND}, estimated by this approach, was related to the amount of released dopamine or to the administered mass of raclopride. We also demonstrated that the reduction in BP_{ND} varied according to the increase in administered raclopride in monkey studies. The proposed method, with multiple injections, has potential for use in quantitatively assessing the change in specific binding, in a short study period, for several neurotransmitter competition studies.

Acknowledgments

This research was supported by the Ministry of Education, Culture, Sports, Science and Technology, Grant-in-Aid for Young Scientists (B) (No.20790839), Japan, Kobe Cluster I and II, Ministry of Education, Culture, Sports, Science and Technology of Japan (MEXT; T.H.), and the MHLW (Ministry of Health, Labour and Welfare of Japan) Health Science Research Grant, H17-025 (T.H., H.I).

We are grateful to members of the Department of Investigative Radiology, National Cardiovascular Center Research Institute, for their support of the PET experiment and for helpful suggestions.

Appendix A

The multiple-injection simplified reference tissue model is based on the following differential equations of the simplified reference tissue model on the assumption that the time–activity curves of the target and reference tissues can be fitted to a single tissue compartment model with plasma input (Lammertsma and Hume, 1996)

$$\frac{dC_t}{dt} = K_1 C_p(t) - k_{2a} C_t(t) \tag{A1}$$

$$\frac{dC_r}{dt} = K_1^r C_p(t) - k_2^r C_t(t) \tag{A2}$$

$$K_1 / k_{2a} = K_1 / k_2 \cdot (1 + \mathrm{BP_{ND}}) \tag{A3}$$

where C_p is the metabolite corrected plasma concentration, C_t and C_r are the concentration in target and reference tissue, respectively, k_{2a} (min^{-1}) is the apparent (overall) rate constant for transfer from specific compartment to plasma in the target tissue.

Eqs. (A1) and (A2) are expressed as follows by Laplace transform:

$$sC_t(s) - C_t(0) = K_1 C_p(s) - k_{2a} C_t(s) \tag{A4}$$

$$sC_r(s) - C_r(0) = K_1^r C_p(s) - k_2^r C_t(s) \tag{A5}$$

where $C_t(0)$ and $C_r(0)$ are the total concentration in target and reference tissue, respectively, at the time of injection.

From Eqs. (A4),(A5) and the assumption $K_1^r / k_2^r = K_1 / k_2$, the following expression can be derived:

$$C_t(s) = R_1 C_r(s) + \frac{1}{s + k_{2a}}(k_2 - Rk_{2a})C_r(s) + \frac{1}{s + k_{2a}}(C_t(0) - R_1 C_r(0)). \tag{A6}$$

From Eqs. (A3) and (A6), the following expression can be derived by inverse-Laplace transform:

$$C_t(t) = R_1 C_r(t) + \left(k_2 - \frac{R_1 k_2}{1 + \mathrm{BP_{ND}}}\right) e^{-\frac{k_2}{1 + \mathrm{BP_{ND}}} t} \otimes C_r(t) + (C_t(0) - R_1 C_r(0)) e^{-\frac{k_2}{1 + \mathrm{BP_{ND}}} t}. \tag{A7}$$

In the second injection, R_1, k_2, and $\mathrm{BP_{ND}}$ can be estimated by giving $C_t(t)$, $C_r(t)$, and $C_t(0)$ and $C_r(0)$ at the time of second injection. Meanwhile, in the first injection, $C_t(0)$ and $C_r(0)$ are 0 at the time of first injection, so $C_t(t)$ can be expressed as follows:

$$C_t(t) = R_1 C_r(t) + \left(k_2 - \frac{R_1 k_2}{1 + \mathrm{BP_{ND}}}\right) e^{-\frac{k_2}{1 + \mathrm{BP_{ND}}} t} \otimes C_r(t). \tag{A8}$$

References

Breier, A., Su, T.P., Saunders, R., Carson, R.E., Kolachana, B.S., de Bartolomeis, A., Weinberger, D.R., Weisenfeld, N., Malhotra, A.K., Eckelman, W.C., Pickar, D., 1997. Schizophrenia is associated with elevated amphetamine-induced synaptic dopamine concentrations: evidence from a novel positron emission tomography method. Proc. Natl. Acad. Sci. U.S.A. 94, 2569–2574.

Carson, R.E., Breier, A., de Bartolomeis, A., Saunders, R.C., Su, T.P., Schmall, B., Der, M.G., Pickar, D., Eckelman, W.C., 1997. Quantification of amphetamine-induced changes in [^{11}C]raclopride binding with continuous infusion. J. Cereb. Blood Flow Metab. 17, 437–447.

Christian, B.T., Narayanan, T., Shi, B., Morris, E.D., Mantil, J., Mukherjee, J., 2004. Measuring the in vivo binding parameters of [18F]-fallypride in monkeys using a PET multiple-injection protocol. J. Cereb. Blood Flow Metab. 24, 309–322.

Delforge, J., Pappata, S., Millet, P., Samson, Y., Bendriem, B., Jobert, A., Crouzel, C., Syrota, A., 1995. Quantification of benzodiazepine receptors in human brain using PET, [^{11}C] flumazenil, and a single-experiment protocol. J. Cereb. Blood Flow Metab. 15, 284–300.

Doudet, D.J., Jivan, S., Holden, J.E., 2003. In vivo measurement of receptor density and affinity: comparison of the routine sequential method with a nonsequential method in studies of dopamine D_2 receptors with [^{11}C]raclopride. J. Cereb. Blood Flow Metab. 23, 280–284.

Endres, C.J., Kolachana, B.S., Saunders, R.C., Su, T., Weinberger, D., Breier, A., Eckelman, W.C., Carson, R.E., 1997. Kinetic modeling of [^{11}C]raclopride: combined PET-microdialysis studies. J. Cereb. Blood Flow Metab. 17, 932–942.

Endres, C.J., Carson, R.E., 1998. Assessment of dynamic neurotransmitter changes with bolus or infusion delivery of neuroreceptor ligands. J. Cereb. Blood Flow Metab. 18, 1196–1210.

Farde, L., Ehrin, E., Eriksson, L., Greitz, T., Hall, H., Hedstrom, C.G., Litton, J.E., Sedvall, G., et al., 1985. Substituted benzamides as ligands for visualization of dopamine receptor binding in the human brain by positron emission tomography. Proc. Natl. Acad. Sci. U.S.A. 82, 3863–3867.

Farde, L., Hall, H., Ehrin, E., Sedvall, G., 1986. Quantitative analysis of D_2 dopamine receptor binding in the living human brain by PET. Science 231, 258–261.

Gallezot, J.D., Bottlaender, M.A., Delforge, J., Valette, H., Saba, W., Dollé, F., Coulon, C.M., Ottaviani, M.P., Hinnen, F., Syrota, A., Grégoire, M.C., 2008. Quantification of cerebral nicotinic acetylcholine receptors by PET using 2-[^{18}F]fluoro-A-85380 and the multiinjection approach. J. Cereb. Blood Flow Metab. 28, 172–189.

Gunn, R.N., Lammertsma, A.A., Hume, S.P., Cunningham, V.J., 1997. Parametric imaging of ligand–receptor binding in PET using a simplified reference region model. Neuroimage 6, 279–287.

Hall, H., Köhler, C., Gawell, L., Farde, L., Sedvall, G., 1988. Raclopride, a new selective ligand for the dopamine-D2 receptors. Prog. Neuropsychopharmacol. Biol. Psychiatry 12, 559–568.

Herzog, H., Tellmann, L., Hocke, C., Pietrzyk, U., Casey, M.E., Kuwert, T., 2004. NEMA NU2-2001 guided performance evaluation of four Siemens ECAT PET scanners. IEEE Trans. on. Nucl. Science 51, 2662–2669.

Ikoma, Y., Toyama, H., Suhara, T., 2004. Simultaneous quantification of two brain functions with dual tracer injection in PET dynamic study. In: Iida, H., Shah, N.J., Hayashi, T., Watabe, H. (Eds.), Quantitation in Biomedical Imaging with PET and MRI. InElsevier, pp. 74–78.

Ikoma, Y., Ito, H., Arakawa, R., Okumura, M., Seki, C., Shidahara, M., Takahashi, H., Kimura, Y., Kanno, I., Suhara, T., 2008. Error analysis for PET measurement of dopamine D_2 receptor occupancy by antipsychotics with [^{11}C]raclopride and [^{11}C] FLB457. Neuroimage 42, 1285–1294.

Kim, K.M., Watabe, H., Hayashi, T., Hayashida, K., Katafuchi, T., Enomoto, N., Ogura, T., Shidahara, M., Takikawa, S., Eberl, S., Nakazawa, M., Iida, H., 2006. Quantitative mapping of basal and vasareactive cerebral blood flow using split-dose ^{123}I-iodoamphetamine and single photon emission computed tomography. Neuroimage 33, 1126–1135.

Koepp, M.J., Gunn, R.N., Lawrence, A.D., Cunningham, V.J., Dagher, A., Jones, T., Brooks, D.J., Bench, C.J., Grasby, P.M., 1998. Evidence for striatal dopamine release during a video game. Nature 393, 266–268.

Koeppe, R.A., Raffel, D.M., Snyder, S.E., Ficaro, E.P., Kilbourn, M.R., Kuhl, D.E., 2001. Dual-[11C]tracer single-acquisition positron emission tomography studies. J. Cereb. Blood Flow Metab. 21, 1480–1492.

Köhler, C., Hall, H., Ogren, S.O., Gawell, L., 1985. Specific in vitro and in vivo binding of 3H-raclopride. A potent substituted benzamide drug with high affinity for dopamine D-2 receptors in the rat brain. Biochem. Pharmacol. 34, 2251–2259.

Lammertsma, A.A., Hume, S.P., 1996. Simplified reference tissue model for PET receptor studies. Neuroimage 4, 153–158.

Lammertsma, A.A., Bench, C.J., Hume, S.P., Osman, S., Gunn, K., Brooks, D.J., Frackowiak, R.S., 1996. Comparison of methods for analysis of clinical [^{11}C]raclopride studies. J. Cereb. Blood Flow Metab. 16, 42–52.

Laruelle, M., Iyer, R.N., al-Tikriti, M.S., Zea-Ponce, Y., Malison, R., Zoghbi, S.S., Baldwin, R.M., Kung, H.F., Charney, D.S., Hoffer, P.B., Innis, R.B., Bradberry, C.W., 1997. Microdialysis and SPECT measurements of amphetamine-induced dopamine release in nonhuman primates. Synapse 25, 1–14.

Logan, J., Fowler, J.S., Volkow, N.D., Ding, Y.S., Wang, G.J., Alexoff, D.L., 2001. A strategy for removing the bias in the graphical analysis method. J. Cereb. Blood Flow Metab. 21, 307–320.

Millet, P., Delforge, J., Mauguiere, F., Pappata, S., Cinotti, L., Frouin, V., Samson, Y., Bendriem, B., Syrota, A., 1995. Parameter and index images of benzodiazepine receptor concentration in the brain. J. Nucl. Med. 36, 1462–1471.

Mintun, M.A., Raichle, M.E., Kilbourn, M.R., Wooten, G.F., Welch, M.J., 1984. A quantitative model for the in vivo assessment of drug binding sites with positron emission tomography. Ann. Neurol. 15, 217–227.

Morris, E.D., Babich, J.W., Alpert, N.M., Bonab, A.A., Livni, E., Weise, S., Hsu, H., Christian, B.T., Madras, B.K., Fischman, A.J., 1996a. Quantification of dopamine transporter density in monkeys by dynamic PET imaging of multiple injections of ^{11}C-CFT. Synapse 24, 262–272.

Morris, E.D., Alpert, N.M., Fischman, A.J., 1996b. Comparison of two compartmental models for describing receptor ligand kinetics and receptor availability in multiple injection PET studies. J. Cereb. Blood Flow. Metab. 16, 841–853.

Muzic, R.R., Nelson, A.D., Saidel, G.M., Miraldi, F., 1996. Optimal experiment design for PET quantification of receptor concentration. IEEE Trans. Med. Imaging 15, 2–12.

Yoder, K.K., Wang, C., Morris, E.D., 2004. Change in binding potential as a quantitative index of neurotransmitter release is highly sensitive to relative timing and kinetics of the tracer and the endogenous ligand. J. Nucl. Med. 45, 903–911.

Watabe, H., Endres, C.J., Breier, A., Schmall, B., Eckelman, W.C., Carson, R.E., 2000. Measurement of dopamine release with continuous infusion of [^{11}C]raclopride: optimization and signal-to-noise considerations. J. Nucl. Med. 41, 522–530.

Watabe, H., Ohta, Y., Teramoto, N., Miyake, Y., Kurokawa, M., Yamamoto, A., Ose, Y., Hayashi, T., Iida, H., 2006. A novel reference tissue approach for multiple injections of [C-11]Raclopride. Neuroimage 31 (Suppl. 2), T73.

Zhou, Y., Chen, M.K., Endres, C.J., Ye, W., Brasic, J.R., Alexander, M., Crabb, AH, Guilarte, TR, Wong, D.F., 2006. An extended simplified reference tissue model for the quantification of dynamic PET with amphetamine challenge. Neuroimage 33, 550–563.

Conceptual Design of High Resolution and Quantitative SPECT System for Imaging a Selected Small ROI of human brain

Tsutomu Zeniya, Yoshiyuki Hirano, Tomonori Sakimoto, Kenji Ishida, Hiroshi Watabe, *Member, IEEE*, Noboru Teramoto, Hiroyuki Kudo, *Member, IEEE*, Kotaro Minato, *Member, IEEE*, Jun Hatazawa, and Hidehiro Iida, *Member, IEEE*

***Abstract*– We designed a concept of high resolution and quantitative SPECT for imaging a selected small region-of-interest (ROI) of human brain. This system is aimed at achieving high resolution less than 1 mm and being applied for imaging neurons and evaluating drug delivery system. Pinhole or cone-beam collimators are useful for high-resolution imaging of small ROI. However, when the ROI is smaller than the object, the projection data are truncated by radioisotope outside ROI. In the reconstructed image, the truncation causes the artifact and the overestimation of voxel value, which deceases quantitative accuracy of physiological functions. We are introducing the new truncation compensated 3D-OSEM (TC-3DOSEM) reconstruction method. The truncated data can be successfully reconstructed within ROI by fulfilling the condition that ROI contains a priori knowledge. In addition to small field-of-view (FOV) detector, we are introducing the parallel-hole collimator attached large FOV detector covering the entire brain, to acquire the non-truncated data and provide the priori knowledge in small ROI, even if the resolution of the detector is low. For imaging with high resolution, we are using $LaBr_3$(Ce) scintilator with optically coupled to position-sensitive photomultiplier tube (H8500, Hamamatsu, Japan) as the detector. And also, for proof of our concept, we performed preliminary experiment using pinhole SPECT and brain phantom. The reconstruction ROI contained the region outside the brain, that is, zero count as the priori knowledge. The truncated data were reconstructed by TC-3DOSEM. The reconstructed image without artifact and overestimation was obtained with high resolution. This preliminary experiment suggested feasibility of high resolution and quantitative SPECT for imaging a selected small ROI of human brain.**

Manuscript received November 13, 2009. This work was supported in part by the Grant-in-Aid for Scientific Research (C) (20500435) of the Ministry of Education, Culture, Sports and Technology (MEXT) , Japan, the Grant for Translational Research from the Ministry of Health, Labour and Welfare (MHLW), Japan, Newly Adopted Projects of Regional R&D Programs for FY2008 from Kansai Bureau of Economy, Trade and Industry, Japan.

T. Zeniya, Y. Hirano, K. Ishida, H. Watabe, N. Teramoto and H. Iida are with the Department of Investigative Radiology, Advanced Medical Engineering Center, National Cardiovascular Center Research Institute, 5-7-1 Fujishirodai, Suita, Osaka 565-8565 Japan (e-mail: zeniya @ri.ncvc.go.jp).

T. Sakimoto and K. Minato with the Graduate School of Information Science, Nara Institute of Science and Technology, Japan.

H. Kudo is with the Department of Computer Science, Graduate School of Systems and Information Engineering, University of Tsukuba, Japan.

J. Hatazawa is with the Department of Nuclear Medicine and Tracer Kinetics, Osaka University Graduate School of Medicine, Japan.

I. Introduction

We designed a concept of high resolution and quantitative SPECT for imaging a selected small region-of-interest (ROI) of human brain. This system is aimed at achieving high resolution less than 1 mm and being applied for imaging neurons and evaluating drug delivery system. Also, for proof of our concept, we carried out preliminary experiment using pinhole SPECT and brain phantom.

II. Conceptual Design

Pinhole or cone-beam collimators are useful for high-resolution imaging of small ROI. However, as shown in Fig. 1, when the reconstruction ROI is smaller than the object like human brain, the projection data are truncated by radioisotope outside ROI. Because of this truncation, the voxel value of the reconstructed image is overestimated. This hampers quantitative assessment of physiological functions.

Recently, Kudo et al proposed reconstruction theory to solve the interior problem in computed tomography (CT) [1]. We are applying it for pinhole and cone-beam SPECT. Let's explain how to realize with Fig. 2. According to Kudo's theory, the truncated data can be successfully reconstructed within ROI by fulfilling the condition that ROI contains a priori knowledge. In addition to small field-of-view (FOV) detector for imaging with high resolution, we are introducing the parallel-hole collimator attached large FOV detector covering the entire brain to acquire the non-truncated data, even if the resolution of the detector is low. As another condition, the reconstruction matrix must be larger than the object.

Figure 3 is a conceptual illustration of high resolution and quantitative SPECT system for imaging a selected small ROI of human brain. This system has two types of detectors. One is pinhole or cone-beam collimator attached $LaBr_3$(Ce) scintillator with high intrinsic spatial resolution of approximately 1 mm [2] for imaging a selected small ROI with high resolution. The other is parallel-hole collimator attached NaI(Tl) scintillator with active area of 250 mm × 150 mm for acquiring the non-truncated data. Position-sensitive photomultiplier tubes (H8500, Hamamatsu, Japan) are optically coupled to both scintilators.

9781-4244-3962-1/09/$25.00 ©2009 IEEE

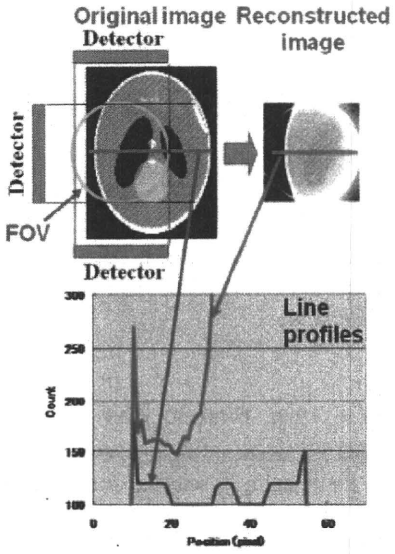

Fig. 1. The artifact and overestimation on the reconstructed image due to truncation.

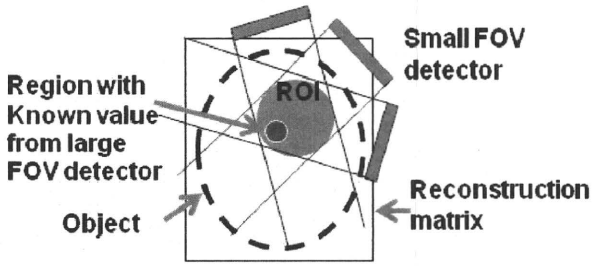

Fig. 2. Schematic diagram showing the solution of the interior problem.

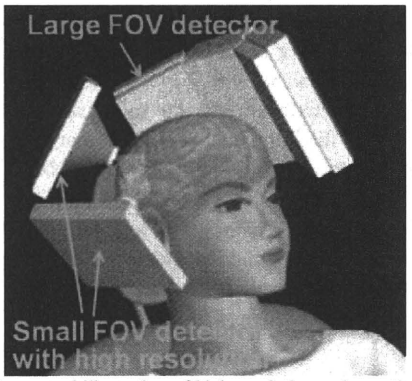

Fig. 3. Conceptual illustration of high resolution and quantitative SPECT system for imaging a selected small ROI of human brain.

III. Preliminary Experiment

For proof of our concept, we performed preliminary experiment using pinhole SPECT and Hoffman brain phantom [3]. The reconstruction ROI contained the region outside the brain, that is, almost zero count as the priori knowledge [4]. The truncated data were reconstructed by truncation compensated 3D-OSEM (TC-3DOSEM) reconstruction method for pinhole SPECT [5].

Figure 4 shows the experimental setup. We scanned a part of Hoffman brain phantom using the rotating stage and 1-mm pinhole collimator fitted to clinical SPECT gamma camera (GCA7200A, Toshiba, Japan). As for the scan parameters, the phantom was filled with Tc-99m of 1,480 MBq and scanned for 2 hours, the radius of rotation was 95mm, the imaging FOV was 95 mm, and the rotation angle was 180 degrees. This radius of rotation is that collimator doesn't hit again the phantom in case of circular orbit and 180 degrees rotation. And also, we scanned same phantom using parallel collimator to compare in terms of spatial resolution.

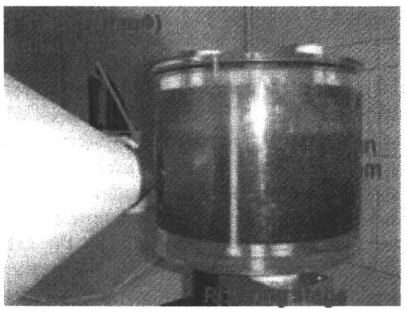

Fig. 4. Experimental setup for scanning Hoffman brain phantom by pinhole SPECT.

Figure 5 shows results of human brain phantom study. In case of clinical SPECT with parallel collimator, the resolution of the reconstructed image was low. In case of pinhole collimator and conventional 3DOSEM, the resolution was high, but the artifact appeared at the edge of ROI and the voxel counts were overestimated. On the other hand, combination of pinhole collimator and TC-3DOSEM provide high resolution image and eliminated the artifact and the overestimation. In this experimental geometry using pinhole collimator, theoretical resolution was approximately 2 mm.

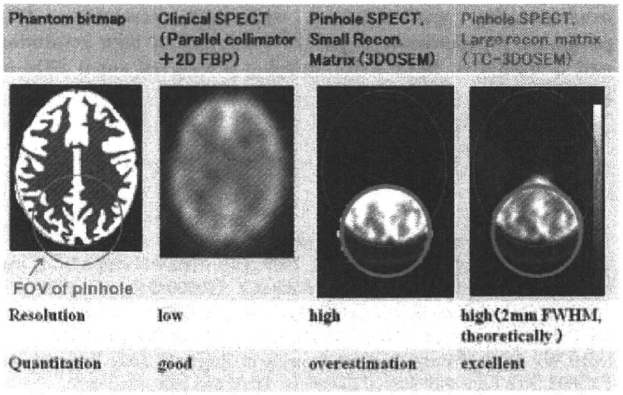

Fig. 5. Comparison of the reconstructed image from preliminary experiment using brain phantom.

IV. Conclusion

We have designed the concept of high resolution and quantitative SPECT for imaging a selected small ROI of human brain. And also, the preliminary experiment suggested

feasibility of high resolution and quantitative SPECT for human brain.

REFERENCES

[1] H. Kudo, M. Courdurier, F. Noo, and M. Defrise, "Tiny a prior knowledge solves the interior problem in computed tomography," *Phys. Med. Biol.*, vol. 53, no. 9, pp. 2207-2231, 2008.

[2] R. Pani, R. Pellegrini, M. N. Cinti, P. Bennati, M. Betti *et al.*, "$LaBr_3$:Ce crystal: The latest advance for scintillation cameras," *Nucl Instrum Meth A.*, vol. 572, pp. 268-269, 2007.

[3] E. J. Hoffman, P. D. Cutler, W. M. Digby, and J. C. Mazziotta, "3D phantom to simulate cerebral blood flow and metabolic images for PET," *IEEE Trans. Nucl. Sci.*, vol. 37, pp. 616-620, 1990.

[4] M. Defrise, F. Noo, R. Clackdoyle, and H. Kudo, "Truncated Hilbert transform and image reconstruction from limited tomographic data," *Inverse Problems*, vol. 22, pp. 1037-1053, 2006.

[5] T. Zeniya, H. Watabe, A. Sohlberg, T. Inomata, H. Kudo, et al., "3D-OSEM reconstruction from truncated data in pinhole SPECT," *2007 IEEE Nuclear Science Symposium Conference Record*, vol. 6, pp. 4205-4207, 2007.

Interior SPECT Reconstruction Problem with Tiny *a proiri* Knowledge – An Application for High Resolution Pinhole Brain Imaging

Qiu Huang, Tsutomu Zeniya, Hiroyuki Kudo, Hidehiro Iida, and Grant T. Gullberg

Abstract— **The quantitation of cerebral blood flow (CBF) and cerebral vascular reactivity (CVR) are valuable in diagnosing brain ischemia, and the quantitation of benzodiazepine receptor density is important in evaluating neuronal damage due to ischemic effects. To better evaluate cerebral autoregulation, a high resolution brain single photon emission computed tomography (SPECT) imager is being built that provides an image of the entire brain for support information in the reconstruction of the interior problem from small field-of-view, truncated projections for high resolution ROI imaging.**

Kudo *et al.* presented a unique and stable solution to the interior problem in computed tomography (CT) given tiny *a proiri* knowledge of the object. In this work we advance their result to the interior reconstruction problem in SPECT where a uniform attenuation map is assumed in brain imaging.

In the theory, differentiation followed by backprojection (DBP) of truncated SPECT data is shown to obtain the truncated weighted Hilbert transform. Then with *a proiri* information on a small part of the region-of-interest (ROI), the other part of the ROI is shown to be available using the projection onto convex sets (PCOS) method. Simulations show that the algorithm provides quantitative results for the reconstruction of the fan-beam tomographic data. Iterative reconstruction of the pinhole data is under investigation to verify the accuracy of the central slice and to provide reasonable results for regions off the central slice.

Index Terms—**interior problem, SPECT, uniform attenuation, brain imaging.**

I. Introduction

The Department of Investigative Radiology at the National Cardiovascular Center Research Institute in Osaka, Japan is designing a high resolution single photon emission computed tomography (SPECT) imager for obtaining high resolution brain scans for various imaging diagnostic applications. The camera consists of one large field of view detector imaging the whole brain and multiple smaller field of view high resolution detectors imaging small regions of the brain (see Fig. 1). The large field of view detector provides images without truncation that localize areas of particular diagnostic interest and provide support information for the reconstruction of high resolution regions of interest (ROIs) from high resolution truncated projections obtained with the small field of view detectors. The work presented in this paper develops an algorithm that accurately reconstructs uniformly attenuated truncated projections, which is an extension of the interior reconstruction problem for the reconstruction of non attenuated truncated projections.

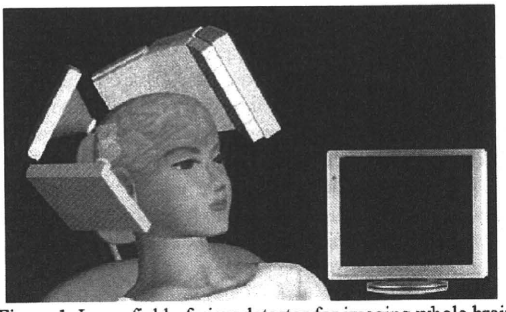

Figure 1. Large field of view detector for imaging whole brain and smaller field of view detectors for imaging ROIs.

The Department of Investigative Radiology has been involved in a large-scale multicenter clinical study aimed at evaluating validity and impact of a quantitative SPECT reconstruction package (QSPECT) [1] for multicenter clinical studies. The quantitative SPECT reconstruction package provides quantitative functional parametric images which are consistent among different setup of equipments and institutions. This allows the use of SPECT in a large scale clinical evaluation for diagnosing brain autoregulatory abnormalities. (A review of noninvasive diagnostic tests to assess cerebral autoregulation can be found in [2].) Dynamic SPECT scans are used to quantify cerebral blood flow (CBF) and cerebral vascular reactivity (CVR) in a single session using a split dose administration of ^{123}I iodo-amphetamine (IMP); one at rest and one during Diamox challenge [3]. Clinical data using QSPECT demonstrated that CBF at rest and during Diamox was reproducible among institutions.

This work was supported in part by the National Institutes of Health under Grant R01 EB00121, and in part by the Director, Office of Science, Office of Biological and Environmental Research, Medical Sciences Division of the U.S. Department of Energy under Contract DE-AC02-05CH11231.

Qiu Huang is with Lawrence Berkeley National Laboratory, One Cyclotron Road, MS 55R0121, Berkeley, CA 94720-8119. (phone: 510-495-2714; fax: 510-486-4768; e-mail: qhuang@lbl.gov).

Tsutomu Zeniya is with the National Cardiovascular Center Research Institute, Suita, Osaka, Japan (e-mail: zeniya @ri.ncvc.go.jp).

Hiroyuki Kudo is with University of Tsukuba, Tsukuba, Japan (e-mail: kudo@*is*.tsukuba.ac.jp).

Hidehiro Iida is with the National Cardiovascular Center Research Institute, Suita, Osaka, Japan (e-mail: iida@ri.ncvc.go.jp).

Grant T. Gullberg is with Lawrence Berkeley National Laboratory, One Cyclotron Road, MS 55R0121, Berkeley, CA 94720-8119. (e-mail: gtgullberg@lbl.gov).

Another important part of the multi-center trial is to evaluate neuronal damage due to ischemia and to provide prognostic value for surgical outcomes. Damage of benzodiazepine receptors has been found in cases of patients with severe brain ischemia [4]. Also, alterations of central benzodiazepine receptors have been described in several neuropsychiatric conditions, including epilepsy, Alzheimer's disease, Huntington's chorea and schizophrenia. Carbon-11-flumazenil, a benzodiazepine antagonist, has been used as a PET radiotracer for visualization and quantification of benzodiazepine receptors in humans. Recently, an iodinated analog of flumazenil, iomazenil has been introduced as a SPECT radiotracer. SPECT imaging of iodine-123-iomazenil (Iomazenil) binding to benzodiazepine receptors in the brain is being used to evaluate neuronal damage caused by ischemia [4] and the prognosis prior to carotid endoarterectomy [5]. Kinetic model-based methods have been developed for SPECT to quantitatively measure ^{123}I-iomazenil binding to benzodiazepine receptors in the human brain [6].

The Department of Investigative Radiology is developing a camera that will perform high resolution imaging of local ROIs in the brain to better address these imaging applications. Imaging with a high resolution small field of view camera provides truncated projections. The reconstruction of these projections involves determining the solution to the interior problem in local tomography. The interior problem in medical imaging refers to the situation where the region-of-interest (ROI) is totally contained within the object. For instance, in SPECT, the interior problem happens when the projections passing through the region outside the ROI are truncated due to a small field-of-view detector or a short detector-to-object distance in the case of converging collimation. The interior problem has been studied for some time [7]. Recently, Kudo *et al.* [8] proved that the solution is unique and stable in computed tomography (CT) if a small region in the ROI is known *a proiri*. In this paper this result is extended to the SPECT interior reconstruction problem.

Both in the work of Kudo *et al.* and in the work presented in this paper, the theory for the solution to the interior problem is based on the differentiation backprojection (DBP) method. The concept of DBP was first developed in parallel beam [9] and cone-beam [10] geometry in CT. The non interior truncation problem was solved for CT in [11], [12], [13], [14], [15]. Similar works in SPECT can be found in [16], [17], [18], [19], [20], where uniform attenuation was assumed. In SPECT the assumption of uniform attenuation is reasonable for some applications such as in brain imaging [21]. The result of the work in this paper shows that, with *a proiri* information of the ROI, the brain image can be reconstructed even when the imaging geometry forms an interior problem. It is expected that this result is useful in the reconstruction of pinhole data, where a pinhole collimator is attached to the small field-of-view cameras for imaging the brain. The pinhole collimator provides a small field-of-view (FOV) with high sensitivity and high resolution when located close to the object.

The paper is organized as follows: Section II shows that the differentiated backprojection (DBP) of fan-beam data is related to the distribution of the radioactive tracer in SPECT through a truncated weighted Hilbert transform. Then a unique inversion is shown to exist for the truncated weighted Hilbert transform given a small region of ROI is known *a proiri*. The results of numerical simulations are presented in Section III where the theory is shown to give a measure of confidence for the quantitative accuracy of the fan-beam reconstruction problem and the conclusion is given in Section IV.

II. METHOD

The method in this work is illustrated by showing that the differentiated backprojection (DBP) of fan-beam data is related to the distribution of the radioactive tracer in SPECT through a truncated weighted Hilbert transform and the truncated weighted Hilbert transform can be inverted given some prior information.

A. DBP operation for fan-beam data

For a transaxial slice, let $f(x,y)$ represent the distribution of the radiopharmaceutical in body tissues, which is assumed to be a smooth and compactly supported function of R^2. The SPECT image reconstruction estimates $f(x,y)$ from the detected photon counts. We denote $\vec{r}=(x,y)$ and $D=\{(x,y)\in R^2:\ x^2+y^2\le 1\}$. We assume $f(x,y)\equiv 0$ outside of D and the attenuation μ of the body tissues is uniform inside D. A typical fan-beam data acquisition geometry with a circular focal-point trajectory is shown in Fig. 2, where each projection ray is represented by (β,σ). One particular projection ray is shown emanating from the focal point S for the angle β with the ray angle σ.

In this paper, the fan-beam uniformly attenuated projection of the function $f(x,y)$ is defined as

$$[D_\mu f](\beta,\sigma)=\int_0^\infty f(S+\tau\vec{\alpha}(\beta,\sigma))e^{\mu\tau}d\tau\,, \qquad (1)$$

where $D_\mu f$ is the projection operator for the uniformly attenuated fan-beam projection data, $\sigma\in[-\sigma_m,\sigma_m]$, and $\vec{\alpha}(\beta,\sigma)$ is a unit vector in R^2 representing the direction from the focal point to the collimation hole, as shown in Fig. 2. Here, $\sigma_m\in(0,\pi/2)$ denotes the maximum angle subtended by the fan-beam. Let R be the radius of the circular focal point trajectory. We can modify the fan-beam data to obtain:

$$g(\beta,\sigma)=e^{-\mu R\cos\sigma}[D_\mu f](\beta,\sigma)\,. \qquad (2)$$

Define

$$s=R\sin\sigma,\quad \theta=\sigma+\beta$$

$$\hat{\sigma}(r,\varphi,\theta)=\arcsin\frac{\vec{r}\cdot\vec{\theta}}{R}=\arcsin\frac{r\cos(\theta-\varphi)}{R}\,.$$

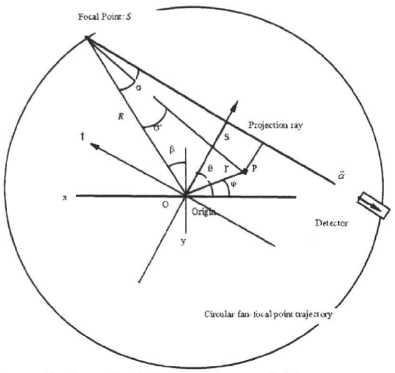

Figure 2. A typical fan-beam acquisition geometry.

We denote $\vec{\theta} = (\cos\theta, \sin\theta)$ and $\vec{\theta}^{\perp} = (-\sin\theta, \cos\theta)$ and construct an image:

$$\hat{f}(x,y) = -\frac{1}{2}\int_{-\pi/2}^{\pi/2} \frac{e^{\mu\vec{r}\cdot\vec{\theta}^{\perp}}[(\frac{\partial}{\partial\sigma} - \frac{\partial}{\partial\beta})g](\theta - \hat{\sigma}(r,\varphi,\theta), \hat{\sigma}(r,\varphi,\theta))}{R\cos\hat{\sigma}(r,\varphi,\theta)} d\theta. \quad (3)$$

This image was proved to be related to the original distribution of radiopharmaceutical as [17]:

$$\hat{f}(x,y) = \int_{-\infty}^{\infty} \frac{\cosh(\mu\tau) f(x-\tau, y)}{\pi\tau} d\tau. \quad (4)$$

Equation (3) involves the operations of derivative and backprojection for the modified attenuated projection in fan-beam geometry and can be readily obtained from fan-beam measurements. Equation (4) shows that the image $\hat{f}(x,y)$ is an image obtained by convolving the true image with a one-dimensional (1D) kernel $\cosh(\mu t)/(\pi t)$ multiplied by some factor, thus the image reconstruction is accomplished by inverting the convolution corresponding to a truncated weighted Hilbert transform.

B. *Inversion of Truncated Hilbert Transform*

Denote the left hand side of (4) by $g(t)$ and the distribution of activity by $f(t)$. The reconstruction is to solve the following integral equation:

$$g(t) = \int_{-1}^{1} \frac{\cosh(\mu\tau) f(t-\tau)}{\pi\tau} d\tau.$$

As shown in Fig. 3, the function $f(t)$ has a support in $-1<t<1$. There is no loss of generality since shifting and scaling can always transform any support interval to $(-1,1)$.

If $g(t)$ is known for $-1<t<1$, the equation can be solved as in [19] and [17]. Unfortunately, for some geometries the function $g(t)$ is only available on a small interval $-1<a<t<d<1$. Then the algorithms in [19] and [17] do not guarantee a stable inversion. However, based on the work by Kudo et al [8], we

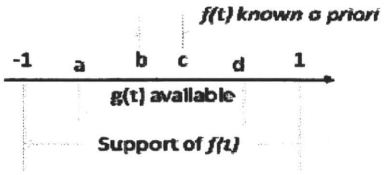

Figure 3. Illustration of intervals.

found if the value of $f(t)$ in the interval $a<b<t<c<d$ is assumed to be known, then the inversion is available in (a,d).

The reconstruction problem becomes:

$$g(t) = \int_{-1}^{1} \frac{\cosh(\mu\tau) f(t-\tau)}{\pi\tau} d\tau \quad . \quad (-1<a<t<d<1), \quad (5)$$

subject to $f(t) = f^{(p)}(t)$ for $(a<b<t<c<d)$.

According to [17], we know the inversion can be obtained by constructing a new function from $g(t)$:

$$\int_{-1}^{1} \frac{g(s)}{\pi(s-t)} \frac{\sqrt{1-t^2}}{\sqrt{1-s^2}} ds.$$

In this case, this function can be broken into two terms: $h_1(t) + h_2(t)$, where

$$h_1(t) = \int_a^d \frac{g(s)}{\pi(s-t)} \frac{\sqrt{1-t^2}}{\sqrt{1-s^2}} ds,$$

$$h_2(t) = \left(\int_{-1}^{a} . + \int_{d}^{1} .\right) \frac{g(s)}{\pi(s-t)} \frac{\sqrt{1-t^2}}{\sqrt{1-s^2}} ds.$$

The first term $h_1(t)$ is available from the truncated weighted Hilbert transform $g(t)$ for $a<t<d$, while the second term $h_2(t)$ remains unknown.

Since the function $f(t)$ is known for $b<t<c$, the second term in this interval can be represented as

$$h_2(t) = \left[\left((I+\Phi)f^{(p)}\right)\right](t) - h_1(t) \qquad \text{for} \qquad t \in (b,c).$$

Here, the operator Φ is the same as in [17] and I indicates the unity operator.

According to the continuity property of analytical functions, the function $h_2(t)$ can be analytically continued from the known interval (b, c) on the real axis to the larger interval (a, d) on the real axis. Since both $h_1(t)$ and $h_2(t)$ are uniquely determined for $t \in (a,d)$, function $f(t)$ is uniquely determined for $t \in (a,d)$. Then the projection onto convex sets (PCOS) method [22] was used to solve the integral equation in (5). Numerical results will be shown in the next section.

III. Numerical Results

In the fan-beam SPECT simulation study, the object image is chosen to be the modified Shepp-Logan phantom shown in Fig. 4. Uniform attenuation coefficient $\mu=0.15cm^{-1}$ was chosen to generate the truncated attenuated fan-beam data.

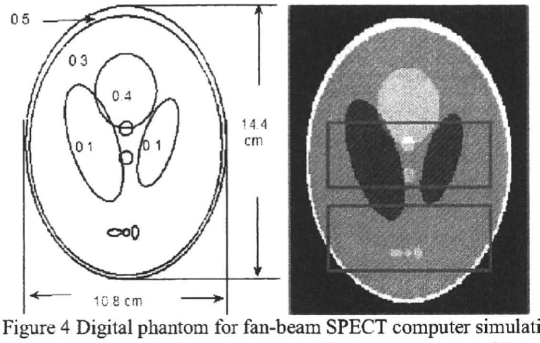

Figure 4 Digital phantom for fan-beam SPECT computer simulation. The square boxes in the right image indicate two regions-of-interest (ROIs).

In the reconstruction, first, differentiation followed by backprojection of truncated SPECT data was obtained. Then assuming the activity within a small part of the region-of-interest is known, the other part of the ROI was estimated using the PCOS method. The reconstructed image is shown in Fig. 5.

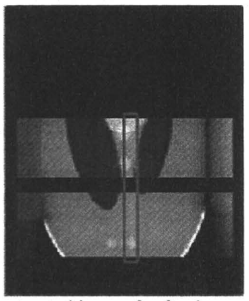

Figure 5: The reconstructed image for fan-beam geometry. The box indicates the region where the distribution is known *a priori.*

IV. Conclusion

This paper extended the work in [8] to SPECT imaging where uniform attenuation map is assumed. The interior problem was shown to be solvable given tiny *a priori* information. Reconstructions from simulated fan-beam data verify the theory.

The investigation of a pinhole system is presently undergoing. In the pinhole simulation, regularized maximum *a posteriori* (MAP) algorithm is used to reconstruct the simulated pinhole data. A low resolution reconstruction of the parallel beam collimated data is used as prior information.

References

[1] Iida H, Hayashida K, Nakazawa M and Katabuchi T, "Multicenter evaluation of quantitative SPECT reconstruction package – QSPECT & DTARG," *J. Nucl. Med.* 47 (Supplement 1), pp. 121, 2006.

[2] Rudzinski W, Swiat M, Tomaszewski M and Krejza J, "Cerebral hemodynamics and investigations of cerebral blood flow regulation," *Nucl Med Rev*, vol. 10, pp. 29-42, 2007.

[3] Imaizumi M, Kitagawa K, Hashikawa K, Oku N, Teratani T, Takasawa M, Yoshikawa T, Rishu P, Ohtsuki T, Hori M, Matsumoto M and Nishimura T, "Misery perfusion with split-dose ^{123}I-iodoamphetamine single-photon emission computed tomography in patients with carotid occlusive diseases," *Stroke*, vol. 33, pp. 2217-2223, 2002.

[4] Moriwaki H, Matsumoto M, Hashikawa K, Oku N, Ishida M, Seike Y, Fukuchi K, Hori M and Nishimura T, "Iodine-123-iomazenil and iodine-123-Iodoamphetamine SPECT in major cerebral artery occlusive disease," *J Nucl Med*, vol. 39, pp. 1348-1353, 1998.

[5] Tsuchida T, Yonekura Y, Sadato N, Takahashi N, Yamamoto K and Ishii Y, "Prediction of improvement of cerebral perfusion with I-123 iomazenil SPECT," *Annals of Nucl. Med.*, vol. 13, pp. 265-268, 1999.

[6] Dargham A, Larulle M, Seibyl J, Rattner Z, Baldwin R M, Zoghbi S S, Zea-Ponce Y, Bremner J D, Hyde T M, Charney D S, Hoffer P B and Innis R B, "SPECT measurement of benzodiazepine receptors in human brain with iodine-123-iomazenil: kinetic and equilibrium paradigms," *J. Nucl. Med.*, vol. 35, pp. 228-238, 1994.

[7] Natterer F, *The Mathematics of Computerized Tomography* (SIAM), 1986.

[8] Kudo H, Courdurier M, Noo F and Defrise M, "Tiny *a proiri* knowledge solves the interior problem in computed tomography," *Phys. Med. Bio.*, vol. 53, pp. 2207-2231, 2008.

[9] Noo F, Clackdoyle R and Pack J D, "A two-step Hilbert transform method for 2D image reconstruction," *Phys. Med. Biol.*, vol. 49, pp. 3903-3923, 2004.

[10] Zou Y and Pan X, "Exact image reconstruction on PI-lines from minimum data in helical cone-beam CT," *Phys. Med. Biol.*, vol. 49, pp. 941-959, 2004.

[11] Pack J D, Noo F and Clackdoyle R, "Cone-beam reconstruction using the backprojection of locally-filtered projections," *IEEE Trans. Med. Imag.*, vol. 24, pp. 70-85, 2005.

[12] Pack J D and Noo F, "Cone-beam reconstruction using 1D filtering along the projection of M-lines," *Phys. Med. Biol.*, vol. 49, pp. 2317-2336, 2004.

[13] Ye Y and Wang G, "Filtered backprojection formula for exact image reconstruction from cone-beam data along a general scanning curve," *Med. Phys.*, vol. 32, pp. 42-48, 2005.

[14] Zou Y and Pan X, "Image reconstruction on PI-lines by use of filtered backprojection in helical cone-beam CT," *Phys. Med. Biol.*, vol. 49, pp. 2717-2731, 2004.

[15] Zou Y and Pan X, "An extended data function and its generalized backprojection for image reconstruction in helical cone-beam CT," *Phys. Med. Biol.*, vol. 49, pp. N3837, 2004.

[16] Huang Q, You J, Zeng G L and Gullberg G T, "Exact Reconstruction From Uniformly Attenuated Helical Cone-Beam projections in SPECT," LBNL Technical Report, LBNL-1359E, Lawrence Berkeley National Lab, Berkeley, USA., 2008.

[17] Huang Q, You J, Zeng G L, and Gullberg G T, "Reconstruction from uniformly attenuated SPECT partial-scan projection data using DBH method," IEEE Trans. Med. Imag., vol. 28, pp. 17-29, 2009.

[18] Noo F and Pack J D, "Theory for image reconstruction from divergent beam projections in SPECT," *IEEE Nuclear Science Symposium Conference Record*, vol. 6, pp. 3449-3452, 2006.

[19] Noo F, Defrise F, Pack J and Clackdoyle R, "Image reconstruction from truncated data in SPECT with uniform attenuation," *Inverse Problems*, vol. 23, pp. 645-667, 2007.

[20] Rullgard H, "An explicit inversion formula for the exponential Radon transform using data from 180 degrees," (Preprint in 2002 Sep) *Ark. Math.*, vol. 42, pp. 353-362, 2004.

[21] Liang Z, Ye J and Harrington D P, "Quantitative brain SPECT in three dimensions: an analytical approach without transmission scans," *Three-Dimensional Image Reconstruction in Radiology and Nuclear Medicine*, Kluwer Academic Publishers, pp. 117-132, 1996.

[22] Youla D C and Webb H, "Image restoration by the method of convex projections: Part I. Theory," *IEEE Trans Med. Imag.*, vol. 1, pp. 81–94, 1982.

Clinical Usability of a Compact High Resolution Detector for High Resolution and Quantitative SPECT Imaging in a Selected Small ROI

Tsutomu Zeniya, Hiroshi Watabe, *Member, IEEE*, Hiroyuki Kudo, *Member, IEEE*, Yoshiyuki Hirano, Kotaro Minato, *Member, IEEE*, and Hidehiro Iida, *Member, IEEE*

Abstract– **SPECT using compact high resolution detector or pinhole collimator allows to image physiological functions with high spatial resolution. However, when field-of-view (FOV) is smaller than the object, the projection data are truncated by radioisotope outside FOV. The truncation causes artifact and overestimation, which decreases quantitative accuracy. Recently Defrise et al proposed a new truncation-compensated reconstruction method, that is, the truncated data can be successfully reconstructed by fulfilling following conditions. First, FOV contains zero or background counts outside the object as known value. Second, reconstructed image space is large enough to contain the whole support of the object. They demonstrated their theory by 2D X-ray CT simulation. This study was aimed at evaluating clinical-SPECT usability of a reconstructed image of a selected small region-of-interest (ROI) with the above Defrise's method. This evaluation was performed by computer simulation with a numerical human brain phantom and a detector with 2-mm resolution, 48-mm FOV and a parallel collimator. The projection data were acquired including the area outside the brain. After adding Gaussian noise, the projection data were reconstructed by maximum likelihood expectation maximization (MLEM) method on the reconstruction matrix large enough to contain the whole support of the brain. This simulation showed that the truncation compensated reconstruction method could provide the image with high resolution and the counts almost equivalent to that of original image in the selected small ROI without the effect of truncation for human brain. In conclusion, this result suggests that a compact high resolution detector can be used for quantitatively reconstructing a selected small ROI with clinical SPECT camera. This technique can also use the pinhole collimator instead of the compact high resolution detector.**

I. Introduction

SPECT using compact high resolution detector or pinhole collimator allows to image physiological functions with high spatial resolution [1]. However, when such a small field-of-view (FOV) detector is applied for a large object like human, the projection data are truncated by radioisotope outside the FOV. The truncation causes artifact and overestimation, which quantitative accuracy. Recently Defrise et al proposed a new truncation-compensated reconstruction method [2]. They demonstrated their theory by 2D X-ray CT simulation. The aim of this study was to evaluate clinical-SPECT usability of a reconstructed image of a selected small region-of-interest (ROI) with the above Defrise's method. This evaluation was performed by 2D computer simulation with a numerical human brain phantom.

II. Materials and Methods

A. Defrise's truncation-compensated reconstruction theory

Defrise's theory compensates the artifact and overestimation due to truncation and exactly reconstructs for FOV, by fulfilling the conditions as shown in Fig. 1. Projection data must be acquired under first condition. And then, the projection data must be reconstructed by iterative reconstruction method such as maximum likelihood expectation maximization (MLEM) method [3] under second condition.

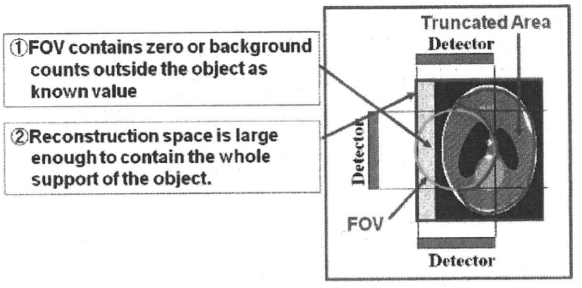

Fig. 1. Conditions to compensated artifact and overestimation due to truncation in Defrise's theory.

B. Computer Simulation

Figure 2 shows the numerical human brain phantom used in this simulation. Image matrix is 90 pixel × 110 pixel. Assuming pixel size of 2 mm, the image size is 180 mm × 220 mm. Pixel values are 1 or 0.

A compact high resolution detector is with 2-mm resolution, 48-mm FOV, 24 bins and a parallel-hole collimator. Projection data for ROI shown by red circle in Fig. 2 were acquired by a circular orbit shown by green line, over 180°,

Manuscript received November 14, 2008. This work was supported in part by the Grant-in-Aid for Scientific Research (B) of the Ministry of Education, Culture, Sports and Technology (20500435), Japan, and the Grant for Translational Research from the Ministry of Health, Labour and Welfare (MHLW), Japan.

T. Zeniya, H. Watabe, Y. Hirano and H. Iida are with the Department of Investigative Radiology, Advanced Medical Engineering Center, National Cardiovascular Center Research Institute, 5-7-1 Fujishirodai, Suita, Osaka 565-8565 Japan (e-mail: zeniya @ri.ncvc.go.jp).

T. Zeniya and K. Minato are with the Graduate School of Information Science, Nara Institute of Science and Technology, Japan.

H. Kudo is with the Department of Computer Science, Graduate School of Systems and Information Engineering, University of Tsukuba, Japan.

978-1-4244-2715-4/08/$25.00 ©2008 IEEE

with 3°step and 60 views. This ROI included the area outside the brain. After adding Gaussian noise, the projection data reconstructed by MLEM method, on the reconstruction matrix of 90 pixel × 110 pixel large enough to contain the whole support of the brain to satisfy the condition of Defrise's theory. To compare with conventional reconstruction method using small reconstruction matrix, projection data with 24 bin were also reconstructed on the reconstruction matrix of 24 pixel × 24 pixel. The number of iteration in MLEM reconstruction was 24 for each method.

To compare with conventional clinical SPECT, untruncated projection data including the whole of the brain were acquired by a 220-mm large FOV (22 bin) detector with low resolution of 10 mm, over 360°, with 3° step and 120 views. After adding Gaussian noise, the projection data were reconstructed by ordered subsets expectation maximization (OSEM) method [4] which is an accelerated MLEM. The OSEM parameters were 8 subsets and 3 iterations.

As reference image, untruncated projection data including the whole of the brain were acquired by a 220-mm large FOV (110 bin) detector with high resolution of 2 mm, over 360°, with 3° step and 120 views. After adding Gaussian noise, the projection data were reconstructed by OSEM method with 8 subsets and 3 iterations. However, this detector is impractical because it is too expensive if manufactured.

The images obtained in this simulation were visually compared, and also the profiles of the images were obtained on line shown by yellow in Fig. 2 to compare quantitatively.

In this simulation, the effects of attenuation, scatter and blurring by collimator were not considered because this simulation was aimed at evaluating truncation-compensated method.

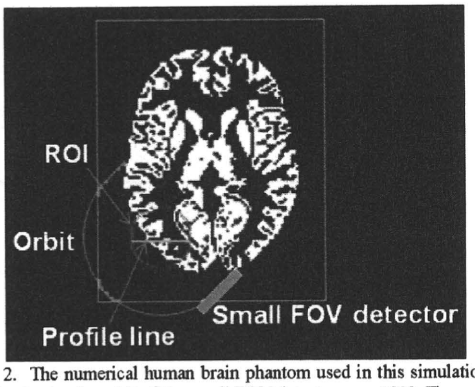

Fig. 2. The numerical human brain phantom used in this simulation. The green line is circular orbit of the small FOV detector over 180°. The red circle is ROI. The yellow line is the position of profiles shown Fig. 4. Pixel values are 1 or 0.

III. Results and Discussion

Figure 3(a) shows the image reconstructed from untruncated projection data using the small FOV detector with low resolution. The obtained image had low resolution. The detail of brain structure was not observed.

Figure 3(b) shows the image reconstructed from untruncated projection data using the large FOV detector with high resolution. The image with high resolution was obtained and the fine structure was observed. However, such a high resolution and large FOV detector is impractical because it is too expensive if manufactured.

Figure 3(c) shows the image reconstructed from truncated projection data obtained using the small FOV detector with high resolution. The projection data were reconstructed on the small reconstruction matrix as conventional reconstruction method. The reconstructed image had artifact and the pixel counts were significantly overestimated.

Figure 3(d) shows the image reconstructed from truncated projection data using the small FOV detector with high resolution. The projection data were reconstructed on the large reconstruction matrix as proposed reconstruction method. The obtained image was with high resolution and the pixel counts almost equivalent to that of original image without the effect of truncation in the selected small ROI.

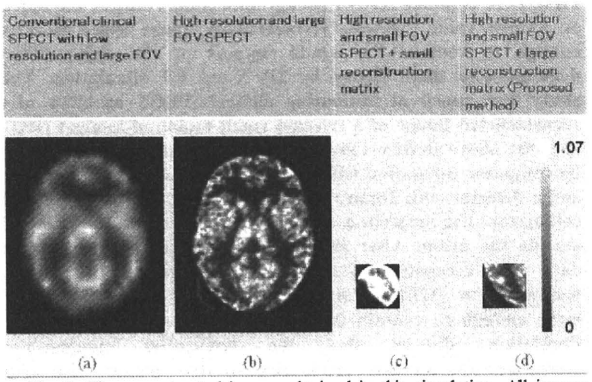

Fig. 3. The reconstructed images obtained in this simulation. All images were displayed with the range of same gray scale [0-1.07] (a) The image obtained from the untruncated projection data of large FOV detector with low resolution as conventional clinical SPECT. (b) The image obtained from the untruncated projection data of large FOV detector with high resolution as the reference image. (c) The image reconstructed from the truncated projection data of small FOV detector with high resolution, on the small reconstruction matrix as conventional reconstruction method. (d) The image reconstructed from the truncated projection data of small FOV detector with high resolution, by the large reconstruction matrix as proposed reconstruction method.

Figure 4 shows the line profiles in a small ROI on the images obtained from the high-resolution detectors. When the truncated projection data from small FOV detector were reconstructed on the small reconstruction matrix, the obtained image had extremely high counts on the edge of and the pixel counts were wholly overestimated. On the other hand, when the truncated projection data from small FOV detector were reconstructed on the large reconstruction matrix, the profile of the image had good agreement with that of the image from the untruncated projection data.

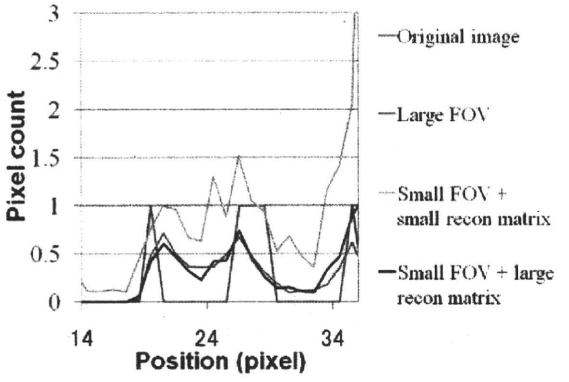

Fig. 4. In a small ROI, the line profiles on the image obtained by reconstructing data from high-resolution detector by each method.

IV. Conclusion

These results suggest that a compact high resolution detector can be used for quantitatively reconstructing a selected small ROI with clinical SPECT camera. This technique can also use the pinhole collimator instead of the compact high resolution detector.

References

[1] S. R. Meikle, P. Kench, M. Kassiou, and R. B. Banati, "Small animal SPECT and its place in the matrix of molecular imaging technologies," *Phys. Med. Biol.*, vol. 50, no. 22, pp. R45-R61, 2005.

[2] M. Defrise, F. Noo, R. Clackdoyle, and H. Kudo, "Truncated Hilbert transform and image reconstruction from limited tomographic data," *Inverse Problems*, vol. 22, no. 3, pp. 1037-1053, 2006.

[3] L. A. Shepp and Y. Vardi, "Maximum likelihood reconstruction for emission tomography," *IEEE Trans. Med. Imaging*, vol. 1, no. 2, pp. 113-122, 1982.

[4] H. M. Hudson and R. S. Larkin, "Accelerated image reconstruction using ordered subsets of projection data," *IEEE Trans. Med. Imaging*, vol. 13, no. 4, pp. 601-609, 1994.

Combination of a High Resolution Detector with Small FOV and a Low Resolution Detector with Large FOV for High Resolution and Quantitative SPECT

Tsutomu Zeniya, Hiroshi Watabe, *Member, IEEE*, Hiroyuki Kudo, *Member, IEEE*, Yoshiyuki Hirano, Kotaro Minato, *Member, IEEE*, and Hidehiro Iida, *Member, IEEE*

Abstract– **SPECT using compact high resolution detector or pinhole collimator allows to image physiological functions with high resolution. However, when region-of-interest (ROI) is smaller than the object, the projection data are truncated due to radioisotope outside ROI. The truncation causes artifact and overestimation, which decrease quantitative accuracy. In theory, to eliminate the artifact and the overestimation due to truncation, the untruncated data from another large field-of-view (FOV) detector can be used even if the detector has low resolution. This study was aimed at evaluating feasibility of combination of a small FOV high resolution detector and a large FOV low resolution detector in clinical circumstance. This evaluation was performed by computer simulation with a numerical torso phantom. We tested whether the image in a selected small ROI (in this case, ROI was heart) can be obtained with high resolution and without artifact and overestimation. The small FOV detector with high resolution was with 1.14-mm resolution, 80-mm FOV and parallel collimator. The whole of heart was included in this FOV, but the surrounding area was truncated. The large FOV detector with low resolution has 9-mm resolution, 360-mm FOV and parallel collimator like conventional clinical SPECT. The untruncated projections including the whole of thorax were acquired by this detector. Gaussian noises were added to all projection data. Data from the small detector were reconstructed by maximum likelihood expectation maximization (MLEM) as iterative method, on the reconstruction matrix large enough to contain the whole of thorax. The reconstructed image from the large FOV detector was used as an initial image in iterative reconstruction. The image obtained by our proposed method had high resolution and the counts almost equivalent to that of original image in the small ROI. In conclusion, this result suggests feasibility of the combination of two detectors with small and large FOV to quantitatively obtain high-resolution image of a selected small ROI with clinical SPECT.**

Manuscript received November 14, 2008. This work was supported in part by the Grant-in-Aid for Scientific Research (B) of the Ministry of Education, Culture, Sports and Technology (20500435) , Japan, and the Grant for Translational Research from the Ministry of Health, Labour and Welfare (MHLW), Japan.

T. Zeniya, H. Watabe, Y. Hirano and H. Iida are with the Department of Investigative Radiology, Advanced Medical Engineering Center, National Cardiovascular Center Research Institute, 5-7-1 Fujishirodai, Suita, Osaka 565-8565 Japan (e-mail: zeniya @ri.ncvc.go.jp).

T. Zeniya and K. Minato are with the Graduate School of Information Science, Nara Institute of Science and Technology, Japan.

H. Kudo is with the Department of Computer Science, Graduate School of Systems and Information Engineering, University of Tsukuba, Japan.

I. Introduction

SPECT using compact high resolution detector or pinhole collimator allows to image physiological functions with high spatial resolution [1]. However, when such a small field-of-view (FOV) detector is applied for a large object like human, the projection data are truncated by radioisotope outside region-of-interest (ROI). The truncation causes artifact and overestimation, which quantitative accuracy. Truncation-compensated reconstruction theory proposed by Defrise et al uses area outside the object with ROI as a prior knowledge to solve the truncation problem [2]. Defrise's theory can't be applied for the case that ROI does not contain the area outside the object. The aim of this study was to evaluate feasibility fo combination of a small-FOV high-resolution detector and a large-FOV low-resolution detector in clinical circumstance. We tested whether the image in a selected small ROI (in this case, ROI was heart) can be reconstructed with high resolution and without the effect of truncation by using untruncated data from the large FOV detector, which do not need to have high resolution, even if ROI in small FOV detector with high resolution does not contain the area outside the object. This evaluation was performed by 2D computer simulation with a numerical human torso phantom.

II. Materials and Methods

A. Support from large-FOV low-resolution detector for truncation problem

As shown in Fig. 1, our proposed method uses untruncated data from the large FOV detector with low resolution, in order to compensate the artifact and overestimation due to truncation in small FOV detector.

Our proposed approach based on iterative reconstruction method such as maximum likelihood expectation-maximization (MLEM) [3] or ordered-subsets expectation-maximization (OSEM) [4] algorithm is, as follows:

Step1: the object is reconstructed using OSEM from untruncated data of the large FOV detector with high resolution;

Step2: In the MLEM reconstruction, the image reconstructed from the large FOV detector is used as initial

978-1-4244-2715-4/08/$25.00 ©2008 IEEE

reference image and forward-projected, and the reconstruction matrix is large enough to contain the whole object;

Step3: Truncated data from small FOV detector are used as real projection in the MLEM reconstruction process.

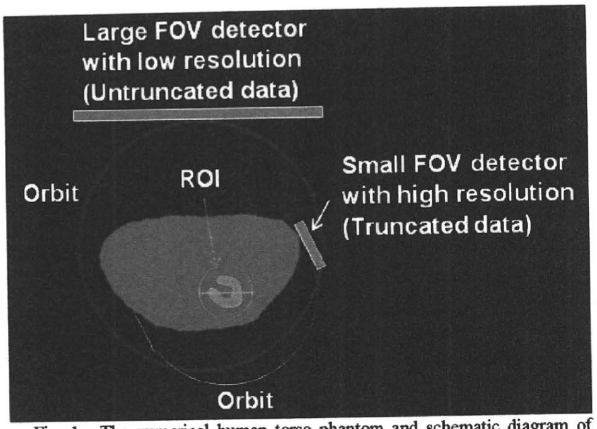

Fig. 1. The numerical human torso phantom and schematic diagram of SPECT system with two kinds of detectors. Untruncated data from low-resolution detector with large FOV are used to compensate the artifact and overestimation due to truncation in small FOV detector. The white line shows the small FOV detector and its circular orbit over 180° to image heart with high resolution. The red line shows the large FOV detector and its circular orbit over 360° to acquire untruncated projection data.

B. *Computer Simulation*

This simulation was performed using the numerical human torso phantom as shown in Fig. 1. Image matrix is 256 pixels × 320 pixels. Assuming pixel size of 1.14 mm, image size 360 mm × 290 mm. Pixel values are 3 and 1 for heart and the surrounding area.

The small FOV detector with high resolution has 1.14-mm resolution, 80-mm FOV and parallel collimator. The whole of heart was included in this FOV, but the surrounding area was truncated. Projection data of ROI shown by white circle in Fig. 1 were acquired by a circular orbit shown by white line, over 180°, with 3°step and 60 views. The large FOV detector with low resolution has 9-mm resolution, 360-mm FOV and parallel collimator like conventional clinical SPECT. The projections data including the whole of thorax were acquired without truncation by this large FOV detector. A red circle in Fig. 1 shows orbit of the large FOV detector. Projection data were acquired with 3° step and 120 views over 360°. Gaussian noises were added to all projection data. Data from the small FOV detector were reconstructed by MLEM method as iterative reconstruction method, on the reconstruction matrix of 256 pixels ×320 pixels large enough to contain the whole of thorax. The reconstructed image from the large FOV detector was used as an initial image in iterative reconstruction. To compare with conventional reconstruction method, projection data with 70 bins were reconstructed on the reconstruction matrix of 70 pixels ×70 pixels. The number of iteration in MLEM reconstruction was 16.

To compare with conventional clinical SPECT, untruncated projection data including the whole of the brain were acquired by a 360-mm FOV (40 bin) detector with low resolution of 9 mm, over 360°, with 3° step and 120 views. After adding Gaussian noise, the projection data were reconstructed by OSEM method as one of iterative reconstruction method, with 8 subsets and 2 iterations.

As reference image, untruncated projection data including the whole of the brain were acquired by a 360-mm FOV (320 bin) detector with high resolution of 1.14 mm, over 360°, with 3° step and 120 views. After adding Gaussian noise, the projection data were reconstructed by OSEM method as one of iterative reconstruction method, with 8 subsets and 2 iterations. However, this detector is impractical because it is too expensive if manufactured.

The images obtained in this simulation were visually compared, and also the profiles of the images were obtained on straight line over heart shown in Fig. 1 to compare quantitatively.

In this simulation, the effects of attenuation, scatter and blurring by collimator were not considered because this simulation was aimed at evaluating truncation-compensated method.

Furthermore, we evaluated the rotating angle in the orbit of small FOV detector. Small rotating angle is desirable because the detector can be closer to the object when the rotating angle is smaller as shown in Fig. 2. Therefore, the small rotating angle improves the sensitivity and the resolution. The rotating angles of 45 °, 90°, 120°, 150° and 180° were tested. All projection data were reconstructed by our proposed method.

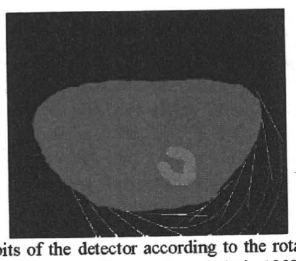

Fig. 2. The orbits of the detector according to the rotating angles. White lines are the orbits of detector. The rotating angle is 180° for the outermost orbit. The rotating angle is 45° for the innermost orbit.

III. Results and Discussion

Figure 3(a) shows the image reconstructed from untruncated projection data using the small FOV detector with low resolution. The obtained image had low resolution. The heart was blurred.

Figure 3(b) shows the image reconstructed from untruncated projection data using the large FOV detector with high resolution. The clear image with high resolution was obtained. However, such a high resolution and large FOV detector is impractical because it is too expensive if manufactured.

Figure 3(c) shows the image reconstructed from truncated projection data obtained using the small FOV detector with high resolution. The projection data were reconstructed on the small reconstruction matrix as conventional reconstruction

method. The reconstructed image had artifact and the pixel counts were significantly overestimated.

Figure 3(d) shows the image reconstructed from truncated projection data using the small FOV detector with high resolution. The projection data were reconstructed by proposed reconstruction method. In the small ROI, the clear image with high resolution was obtained without the artifact and the overestimation, and was almost equivalent to the image from the large FOV detector with high resolution.

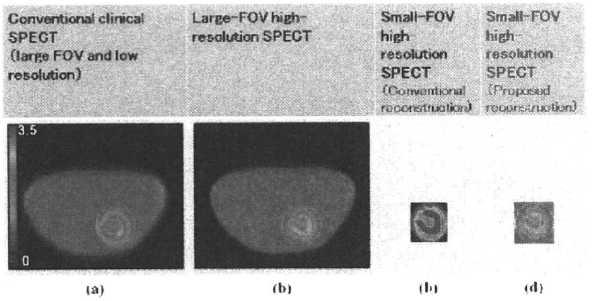

Fig. 3. The reconstructed images obtained in this simulation. All images were displayed with the range of same gray scale [0-3.5] (a) The image obtained from the untruncated projection data of large FOV detector with low resolution as conventional clinical SPECT. (b) The image obtained from the untruncated projection data of large FOV detector with high resolution as the reference image. (c) The image reconstructed from the truncated projection data by small FOV detector with high resolution, on the small reconstruction matrix as conventional reconstruction method. (d) The image reconstructed from the truncated projection data of small FOV detector with high resolution, by proposed reconstruction method.

Figure 4 shows the line profiles in a small ROI on the images obtained from the high-resolution detectors. When the truncated projection data from small FOV detector were reconstructed on the small reconstruction matrix, the obtained image had extremely high counts on the edge of ROI and the pixel counts were wholly overestimated. On the other hand, when the truncated projection data from small FOV detector were reconstructed by our proposed method, the profile of the image had good agreement with that of the image from the untruncated projection data.

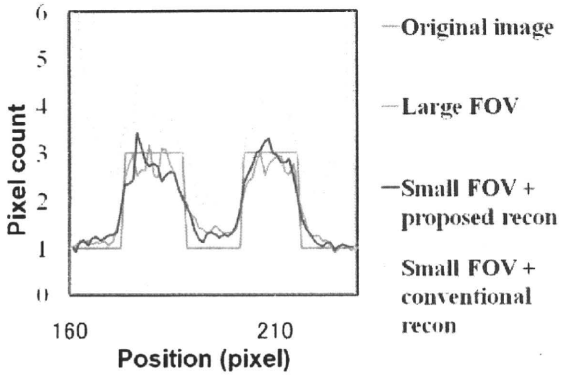

Fig. 4. In a small ROI, the line profiles on the image obtained by reconstructing data from high-resolution detector by each method.

Figure 5 shows the images obtained from projection data acquired by various rotating angles. The image by rotating angle of 150° was almost equivalent to that by rotating angle of 180°. However, the shapes of the hearts were distorted in the images by the rotating angles less than 120°. Usability of the rotating angle of 150° was suggested instead of 180°

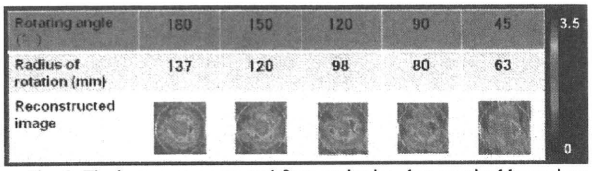

Fig. 5. The images reconstructed from projection data acquired by various rotating angles. When the rotating angle is smaller, the radius of rotation can be smaller.

IV. Conclusion

These results suggested feasibility of the combination of two kinds of detectors with small and large FOVs quantitatively obtain high resolution image of a selected small ROI with clinical SPECT. In other words, the image in a selected small ROI can be reconstructed with high resolution and without the effect of truncation by using untruncated data from the large FOV detector, which do not need to have high resolution, even if ROI in small FOV detector with high resolution does not contain the area outside the object.

References

[1] S. R. Meikle, P. Kench, M. Kassiou, and R. B. Banati, "Small animal SPECT and its place in the matrix of molecular imaging technologies," *Phys. Med. Biol.*, vol. 50, no. 22, pp. R45-R61, 2005.

[2] M. Defrise, F. Noo, R. Clackdoyle, and H. Kudo, "Truncated Hilbert transform and image reconstruction from limited tomographic data," *Inverse Problems*, vol. 22, no. 3, pp. 1037-1053, 2006.

[3] L. A. Shepp and Y. Vardi, "Maximum likelihood reconstruction for emission tomography," *IEEE Trans. Med. Imaging*, vol. 1, no. 2, pp. 113-122, 1982.

[4] H. M. Hudson and R. S. Larkin, "Accelerated image reconstruction using ordered subsets of projection data," *IEEE Trans. Med. Imaging*, vol. 13, no. 4, pp. 601-609, 1994.

トランスレーショナルリサーチを支援する

遺伝子医学 MOOK 9

Gene & Medicine

ますます広がる 分子イメージング技術

生物医学研究から創薬,先端医療までを支える 分子イメージング技術・DDSとの技術融合

別　刷

株式会社 メディカルドゥ